J|A|C|S COMMUNICATIONS

Published on Web 08/16/2010

Reconstruction of Conjugated Oligoelectrolyte Electron Injection Layers

Zhao Chen,[†] Xuan-Dung Dang,[†] Andrea Gutacker,[†,‡] Andrew Garcia,[†] Huaping Li,[†] Yunhua Xu,[†] Lei Ying,[†] Thuc-Quyen Nguyen,[†] and Guillermo C. Bazan*[,†]

Center for Polymers and Organic Solids, Department of Chemistry and Biochemistry, Department of Materials, and Department of Physics, University of California, Santa Barbara, California 93106, and Macromolecular Chemistry Group and Institute for Polymer Technology, Bergische Universität Wuppertal, Gauss-Str. 20, D-42097 Wuppertal, Germany

Received March 18, 2010; E-mail: bazan@chem.ucsb.edu

Abstract: Surface reconstruction of electron injection layers based on conjugated oligoelectrolytes atop an electroluminescent layer occurs in the presence of air. The proposed mechanism involves hydration and concomitant increase of the interfacial energy with the underlying hydrophobic surface followed by dewetting via a nucleation process. No such changes are observed in the case of a conjugated polyelectrolyte, presumably because the lower mobility of the polymer chains leads to a kinetically locked bilayer.

Understanding the factors that influence interface morphology within multilayer organic semiconducting devices is essential for understanding how best to integrate molecular or polymeric materials into various optoelectronic technologies.[1] One particular challenge arises at metal/organic interfaces, where barriers to charge injection can raise the operational voltages of polymer light-emitting diodes (PLEDs) and thin-film transistors and restrict the choice of electrodes. Thin films of conjugated oligoelectrolytes (COEs) have recently found use as electron injection/transport layers (ETLs).[2,3] Electron injection is thought to be facilitated by the formation of a self-assembled dipole layer with the correct orientation for modifying the effective work function of the cathode.[4] Incorporation of the COE has the net effect of lowering the power consumption and opens the opportunity to use environmentally stable electrodes.

Controlling the COE ETL thickness is important for attaining the desired improvement. A similar situation is found in the case of conjugated polyelectrolytes (CPEs), i.e., structures with a larger number of repeat units.[5] If the films are sufficiently thick, ion motion can occur, which redistributes the electric field within the internal structure of the device and gives rise to response times that can be on the order of seconds.[6] Characterization of PLEDs with COE layers between electrodes by atomic force microscopy (AFM) under air revealed a complex surface topography, which becomes smoother closer to the metal contact. These features were originally explained in terms of surface reconstruction due to local heating upon metal deposition.[2a] However, the absence of a precise understanding of the COE ETL structural characteristics and their evolution as a function of processing history prevents the design of improved materials and understanding the mechanism for facilitating injection.

In this contribution, we show that surface reconstruction is a dewetting process due to hydration of the ionic layer. Similar dewetting is not observed with CPEs. Scheme 1 shows the molecular structures of the COE and CPE materials used in our studies, namely, **FPF-BIm$_4$** and **PFN-BIm$_4$**, respectively. Both materials contain tetrakis(1-imidazolyl)borate counteranions. Also shown is a schematic of a typical PLED test structure that highlights the layout of electrodes on the surface and the vertical organization. These devices were fabricated as previously reported and display performance characteristics similar to those in the literature.[2a] Poly[2-methoxy-5-(2′-ethylhexyloxy-1,4-phenylenevinylene)] (MEH-PPV) was chosen as the light-emitting layer and was spin-coated from toluene onto indium tin oxide (ITO) substrates modified with a 60 nm layer of poly(ethylenedioxythiophene):poly(styrenesulfonic acid) (PEDOT:PSS). A layer of **PFN-BIm$_4$** or **FPF-BIm$_4$** was then spin-coated from methanol, after which Al was deposited at 10^{-6} Torr.

Scheme 1. Device Configuration and Molecular Structures

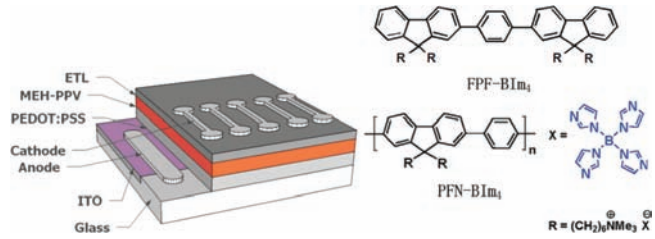

From Figure 1, the topographic features obtained by AFM *under air* show a rougher surface for **FPF-BIm$_4$** than for **PFN-BIm$_4$**. The maximum heights are 16 nm on the **PFN-BIm$_4$** surface and 152 nm on **FPF-BIm$_4$**. Correspondingly, the root-mean-square (rms) roughness increases from ∼0.5 to ∼22 nm.

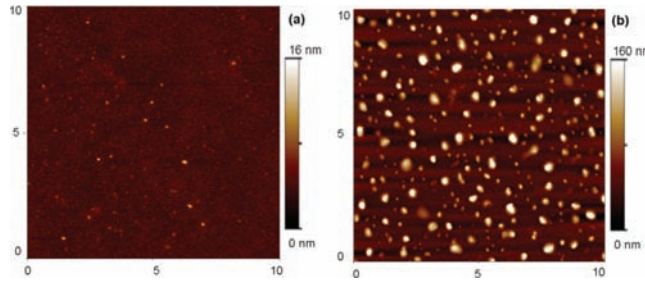

Figure 1. Topographic AFM images of (a) **PFN-BIm$_4$** and (b) **FPF-BIm$_4$** atop an MEH-PPV layer. The size of the images is 10 μm × 10 μm.

Figure 2 shows the surface features upon scanning across the organic/electrode boundary. For this experiment, a ∼1 nm layer of Al was deposited through a mask atop **FPF-BIm$_4$** before examination under air. The left-hand side corresponds to the exposed organic layer, where raised features similar to those in Figure 1b are

[†] University of California.
[‡] Bergische Universität Wuppertal.

10.1021/ja1056856

observed. The electrode surface shown on the right side of the image is smooth. In another experiment, ~1 nm of Al was deposited atop an **FPF-BIm$_4$** layer with characteristics similar to those in Figure 1b. Subsequent examination revealed that Al deposition does *not* significantly modify the topography [see the Supporting Information (SI)]. Therefore, once preformed, the raised features on the film are not modified by cathode deposition.

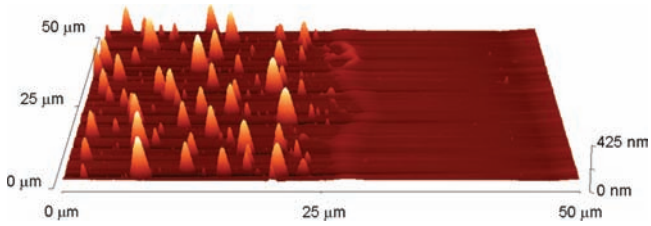

Figure 2. Topographic AFM image of MEH-PPV/**FPF-BIm$_4$**/Al across the Al/organic boundary. The image size is 50 μm × 50 μm.

On the basis of the above observations, it seemed appropriate to examine other effects, in particular exposure to air. To follow the progression of structural properties in a systematic fashion, the MEH-PPV/**FPF-BIm$_4$** surface was scanned inside a cell into which air having a humidity of 18 ± 3 g/m^3 could be introduced for a given period of time and subsequently removed by flushing with Ar. A flow of Ar was otherwise maintained through the cell. A major advantage of this approach is that the same area could be scanned repeatedly by the AFM tip.

Changes in surface features as a function of contact time with moist air are provided in Figure 3. In comparison with the image in Figure 1b, the MEH-PPV/**FPF-BIm$_4$** surface that was kept under Ar shows a smoother topography, with maximum heights of 15 nm (Figure 3a). After 2 min, one observes the appearance of several pin holes throughout the surface; the rim area around these pin holes becomes higher than the surroundings. The holes grow in size with exposure to the air, and the height of the ring edges also increases. In the final image shown in Figure 3d, the holes have connected with each other, and these ribbons decompose to give rise to dropletlike features similar to those in Figure 1b.[7] It is

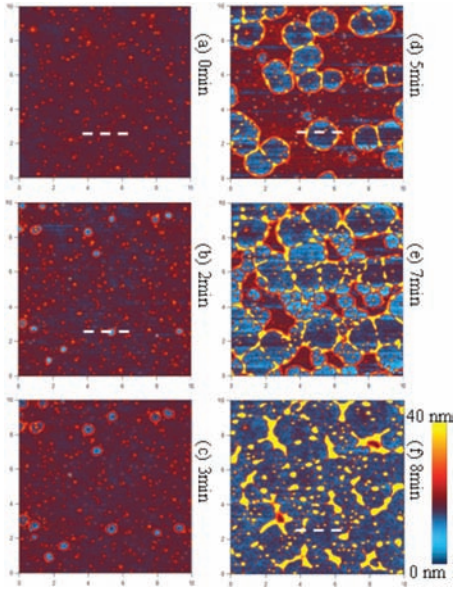

Figure 3. Topographic AFM images (10 μm × 10 μm) of a MEH-PPV/**FPF-BIm$_4$** surface upon contact with moist air for (a) 0, (b) 2, (c) 3, (d) 5, (e) 7, and (f) 8 min.

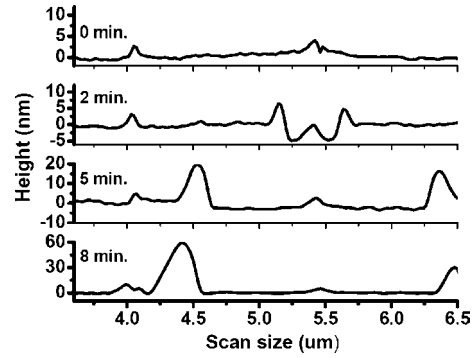

Figure 4. Cross-section lines of images shown in Figure 3.

important to reemphasize that these changes in morphology take place only in the presence of moist air.

AFM cross-sectional analysis provides complementary insight (Figure 4). We chose to examine contact times of 0, 2, 5, and 8 min. The cross-section position (marked in Figure 3 by the white dashed lines) allows us to observe that pin holes initiate and propagate from an initially raised feature. As the top layer of the film peels away from the surface, the adjacent peaks grow in height, consistent with conservation of mass, while the initial raised feature that seeds nucleation remains fixed in its location. Consistent with this process, we found that the roughness of the exposed new surface (0.46 nm) is nearly identical to that of a pristine MEH-PPV surface (0.46 nm).

Finally, we point out that dewetting leads to a progressive deterioration in device performance. As shown in the SI, there is a steady decline in the luminance efficiency (cd/A) as a function of applied bias. A smooth and homogeneous COE layer thus is necessary for achieving optimal results.

The collected set of observations indicates that moisture induces dewetting of the **FPF-BIm$_4$** layer. This process needs to be avoided for optimal PLED performance. Water adsorption as a function of molecular structure is well-understood in CPEs,[8] and this process increases the interface instability with the underlying hydrophobic MEH-PPV. Figure 2 shows that the Al cathode inhibits this process. It is worth pointing out that an **FPF-BIm$_4$** layer atop the more polar PEDOT:PSS remains smooth, even when kept under air (see the SI). Figures 3 and 4 indicate that dewetting proceeds via nucleation (instead of spinoidal decomposition) and propagation from an initial instability, which may be attributed to surface roughness on the underlying MEH-PPV.[9] Thin films of **PFN-BIm$_4$** do not rupture, despite its anticipated similar water absorption and ensuing interfacial instability. Our current thinking is that the decreased mobility of the polymer chains leads to a bilayer that is kinetically locked from detachment.[10] These findings provide a more complete picture of the micro- and nanostructural features of injection layers based on COEs and CPEs and point to the potential advantage of using structurally more stable thin films based on polymeric systems. We also recognize opportunities to create nanoscale patterns via nucleation at specific sites.[11]

Acknowledgment. The authors acknowledge support by MC-CAM, the NSF DMR Program, and the DOE (DE-SC0002368).

Supporting Information Available: Experimental procedures and additional AFM images. This material is available free of charge via the Internet at http://pubs.acs.org.

References

(1) Kahn, A.; Koch, N.; Gao, W. Y. *J. Polym. Sci., Part B: Polym. Phys.* **2003**, *41*, 2529.

(2) (a) Yang, R.; Xu, Y.; Dang, X.-D.; Nguyen, T.-Q.; Cao, Y.; Bazan, G. C. *J. Am. Chem. Soc.* **2008**, *130*, 3282. (b) Xu, Y.; Yang, R.; Peng, J.; Mikhailovsky, A. A.; Cao, Y.; Nguyen, T.-Q.; Bazan, G. C. *Adv. Mater.* **2009**, *21*, 584.
(3) Liu, G.; Li, A. Y.; An, D.; Wu, H. B.; Zhu, X. H.; Li, Y.; Miao, X. R.; Deng, W. L.; Yang, W.; Cao, Y.; Roncali, J. *Macromol. Rapid Commun.* **2009**, *30*, 1484.
(4) (a) Wu, H.; Huang, F.; Mo, Y.; Yang, W.; Wang, D.; Peng, J.; Cao, Y. *Adv. Mater*. **2004**, *16*, 1826. (b) Wu, H.; Huang, F.; Peng, J.; Cao, Y. *Org. Electron.* **2005**, *6*, 118. (c) Seo, J.; Gutacker, A.; Walker, B.; Cho, S.; Garcia, A.; Yang, R.; Nguyen, T.-Q.; Heeger, A. J.; Bazan, G. C. *J. Am. Chem. Soc.* **2009**, *131*, 18220.
(5) Jiang, H.; Taranekar, P.; Reynolds, J. R.; Schanze, K. S. *Angew. Chem., Int. Ed.* **2009**, *48*, 4300.
(6) Hoven, C.; Yang, R.; Garcia, A.; Heeger, A. J.; Nguyen, T.-Q.; Bazan, G. C. *J. Am. Chem. Soc.* **2007**, *129*, 10976.
(7) Reiter, G. *Phys. Rev. Lett.* **1992**, *68*, 75.
(8) Ortony, J. H.; Yang, R.; Brzezinski, J. Z.; Edman, L.; Nguyen, T.-Q.; Bazan, G. C. *Adv. Mater.* **2008**, *20*, 298.
(9) Seemann, R.; Herminghaus, S.; Jacobs, K. *Phys. Rev. Lett.* **2001**, *86*, 5534.
(10) For a polyelectrolyte that detaches upon immersion into an aqueous medium, see: Zhang, J.; Fredin, N. J.; Lynn, D. M. *Langmuir* **2007**, *23*, 11603.
(11) He, X. M.; Winkel, J.; Huck, W. T. S. *Adv. Mater.* **2009**, *21*, 2083.

JA1056856